2026 IEEE International Conference on Robotics and Automation (ICRA 2026)
June 1-5, 2026. Vienna, Austria

Design and Evaluation of a Variable Stiffness Module for an Open-end Tendon Antagonistic Actuator

L. Laohaphand and E. Pengwang

Abstract— **This paper presents a lever mechanism-based Variable Stiffness Module (VSM) for distal joints in physical Human–Robot Interaction (pHRI) robotics applications. Conventional lever mechanism-based VSA designs rely on bulky pivot-regulation mechanisms in an independent motor setup, resulting in high inertia that limits safe pHRI operation. We introduce a novel pivot-regulation mechanism, the Coupled Dual Slider Crank Mechanism (CDSCM), which integrates an antagonistic Twisted String Actuator (aTSA) with the lever mechanism. This method allows smaller actuators to handle a higher load and regulate the pivot from the distal position while preserving the lever mechanism's wide stiffness range ($0 - \infty$ Nm/rad, theoretically) and reducing the weight of the VSM to 0.5 kg. A stiffness model is established to study the torque–deflection relation. The internal force relations of the CDSCM are formulated to guide motor selection. Experiments on pivot regulation demonstrate that the CDSCM can regulate pivots from 0 to 73% of the active range under 1.0 Nm external torque within 0.618 seconds. Actual torque and estimated torque profile are compared in the torque-deflection identification experiment. The maximum achievable stiffness of the VSM is 99.26 Nm/rad, which indicates the design rigidity issues. We address this issue by introducing empirical gain in the torque-deflection model to increase the model accuracy and analyze the VSM design via the SolidWorks static analysis (FEA) to identify the parts that over-deflected under the external load.**

I. INTRODUCTION

Variable Stiffness Actuators is an actuator embedding the adjustable passive joint compliance between the motor and the link's inertia. Passive joint compliance offers three key advantages: 1) reduced development cost, as high-performance force/torque sensors are not required; 2) the ability to generate explosive motion by storing and releasing the spring's elastic energy; and 3) protection of the joint and humans during environmental impacts. It has been theoretically and experimentally demonstrated that to utilize the effect of passive compliance for human safety purposes, the reflected link inertia must be significantly lower than the subject inertia [1], [2], [3], [4]. This is challenging for our targeted application, a robot having a distal joint such as knee/elbow exoskeleton, robotic manipulator, and robotic legs. Also, the inertia, the actuator stiffness range, allowable deflection, stiffness variation speed, size, and weight must be considered, as these directly affect shock absorption and stiffness modulation performance of the VSA [5], [6].

Lattawat Laohaphand and Eakkachai Pengwang are at the Insititute of FIeld roBOtics (FIBO), King Mongkut's University of Technology Thonburi (KMUTT), Bang Mod, Thung Khru, Bangkok, Thailand lattawat.laohap@mail.kmutt.ac.th, eakkachai.pen@kmutt.ac.th

The VSA design guideline are discussed in [5], [7]. Generally, VSA consists of two main modules, Actuation Module (AM) and a Variable Stiffness Module (VSM). The AM consists of two motors for actuating two degree-of-freedom in a joint and can be arranged in antagonistic motor setup or independent motor setup, affecting power consumption and control strategy. The VSM is classified into three group regarding their stiffness modulation method [7]. The outstanding features of each method are summarized as follows:

1) *Changing nonlinear spring preload*: lightweight, compact, high deflection range, high efficiency
2) *Adjusting the transmission ratio between the load and spring (lever mechanism)*: large stiffness adjusting range, lightweight, compact, low energy consumption, high output torque
3) *Modifying the physical properties of the spring*: large stiffness adjusting range, high deflection range, low energy consumption, high output torque

The antagonistic Twisted String Actuator (aTSA) is a lightweight VSA concept which consisting of two Twisted String Actuators (TSA) connected at each open end to form an antagonistic motor setup [8], [9]. They utilize the inherent compliance of the string to perform the stiffness variation, making the design very simple and light. Twisted String Actuators (TSA) are open-end tendon actuators where strings are rotated by motor to transmit a power in translational manner. TSA offer several advantages, including high power-to-weight ratio compared to others transmission system, simple mechanism, nonlinear compliancy depending on the the string parameters, and low cost. However, their nonlinear transmission profile, durability issues, and limited power transmission are major concerns in system implementation. TSAs have been used in various pHRI wearable assistive devices, e.g., hip exoskeleton [10] and bidirectional elbow skeleton [11]. The LVSA introduced in [12] represents a cable-driven lightweight VSA based on a novel spring preloading mechanism, the Four Sliders on a Shared Crank (FS2C). This approach offers structural simplicity, facilitates remote actuator placement, and enables the simultaneous preloading of multiple springs, thereby extending the torque capacity over the conventional spring preloading designs, which typically rely on a single elastic element. The system could achieve a stiffness range of 0 to 988 Nm/rad with a joint weight of 0.412 kg. However, the independent motor configuration necessitates a large, high-power actuator to sustain the spring preload, which substantially increases the

overall system weight. In [13], they proposed the SVSA-II, utilizing the Archimedean Spiral Relocation Mechanism (ASRM) instead of the conventional rack-and-pinion or ball screw method to relocate the pivots of a lever mechanism-based VSM, leading to a very simple and lightweight design. A double-track lever mechanism was also introduced to enhance elastic energy storage and expand the deflection range of the lever system. With this configuration, the design achieved an ideal stiffness range of $0 - \infty$ Nm/rad, a joint weight of 0.867 kg, and a less power consume for stiffness regulation. However, the design relies on an independent motor configuration, which requires a motor to be mounted directly on the VSM, significantly increasing system inertia when operated at distal joints.

To fill the gaps of previous designs, we approach this problem by integrating the lever mechanism VSM with antagonistic Twisted String Actuator, allowing to relocate all actuators to the base, employ smaller motors to handle the load and regulate the pivot, and have a wide stiffness range. In this work, we propose and evaluate a novel pivot-regulating mechanism, the Coupled Dual Slider Crank Mechanism (CDSCM), designed to operate with the antagonistic open-end tendon actuators and a double-track lever mechanism. The key contributions of this article are summarized as follows:

1) Mechanical design detail of a novel pivot-regulating mechanism, CDSCM, which converts antagonistic pulling from open-end tendon actuators into pivot motion within a lever slot. The performance of this mechanism is validated through pivot position regulation experiment using a fabricated prototype.
2) Implementation of a double-track lever mechanism concept, including stiffness modeling and experimental evaluation of the torque–deflection profile using a real prototype.

The rest of this article is organized as follows. Section II presents the conceptual idea and mechanical design of the VSM. Section III provides the mathematical background of the designed mechanism. Sections IV and V describe the experimental setup and discuss the results, respectively. Lastly, the conclusion is given in Section VI.

II. VARIABLE STIFFNESS MODULE DESIGN

This design aimed to achieve four main objectives: 1) Relocate all actuators away from the joint using antagonistic open-end tendon actuators; 2) Employ the lever mechanism as the passive compliance element in the Variable Stiffness Module; 3) Regulate the lever mechanism pivots via antagonistic pulling action; and 4) Minimize the weight and size of the VSM while keeping development cost as low as possible.

A. Conceptual Ideals

In this design, the independent motor configuration of the conventional lever-based VSA is replaced with an aTSA setup. This relocates all actuators away from the joint, generates sufficient pivot-regulation forces using compact motors, and achieves a cost-effective and lightweight actuation unit. The TSA has many design variations depending on the chosen design parameters and implementation techniques, as shown in [14], [15]. Due to the need for sufficient pulling force to regulate the pivot, we adopt a two-string single-bundle TSA configuration without a separator.

The lever mechanism and pivot regulation mechanism are designed in parallel to achieve a compact layout while maximizing energy storage capability and deflection range. The lever mechanism is a pivot-regulated type, inspired by [13], which increases the elastic energy storability by the kinematics of the symmetric double-track layout. Pivots are regulated using two slider-crank mechanisms on the VSM base. Each pivot motion is defined by a slot-pin joint at its input link and a slider support attached to the VSM base. The motion of both pivots is synchronized by combining two separate input links together by using the couple link and shared crank. Because the pivot regulation mechanism offsets the pivot locations from the centerline, the lever mechanism layout is modified to satisfy this constraint. The VSM can achieve an ideal stiffness range from 0 to ∞ Nm/rad through the lever mechanism. The basic principle of the lever mechanism is explained in [7].

B. Mechanical Design

The kinematic diagram and components of an offset lever mechanism in the initial condition are shown in Fig. 1(a). The mechanism consists of two levers, two pivots, two force points, and two joint springs. The external load (τ_{ext}) interacts with the VSM output link and is transmitted through each of connected revolute joints (force point) on the lever, causing each of the lever to rotate around the pivot and deflect the joint spring on the other side. The motion of the joint spring is guided by a slider (customized miniature journal linear bushing), attached with the output link. The lever is milled as a slot, allowing the pivot head to move within it. The slider pin also shares the tail part of the lever slot, requiring the initial pivot position to be offset. Due to the kinematic relationships in the offset lever mechanism, the joint spring on the compressing side deflects more than that on the tensioning side ($\Delta x_c(p,q) > \Delta x_t(p,q)$), as shown in Fig. 2(a). In this prototype however, the spring and slider on the tensioning side have not been connected yet. The design parameters d_1, d_2, and d_3 can be tuned based on the selected spring specifications, including required joint deflection and joint size. The current parameters are preliminary and will require further study to maximize the elastic potential energy per VSM volume.

The CDSCM schematic is depicted in Fig. 1(b), consisting of two input links, two coupled links, two pivots, three linear sliders, and a VSM base. Each input link consists of a TSA mount, a linear spring mount, a coupled link mount, and a torsional spring, which together generate a resultant torque (τ_{in}) around the revolute joint. This torque is converted into a pivot force via the slot–pin joint and the guiding slider, where the pivot body acts as the pin and the guiding slider

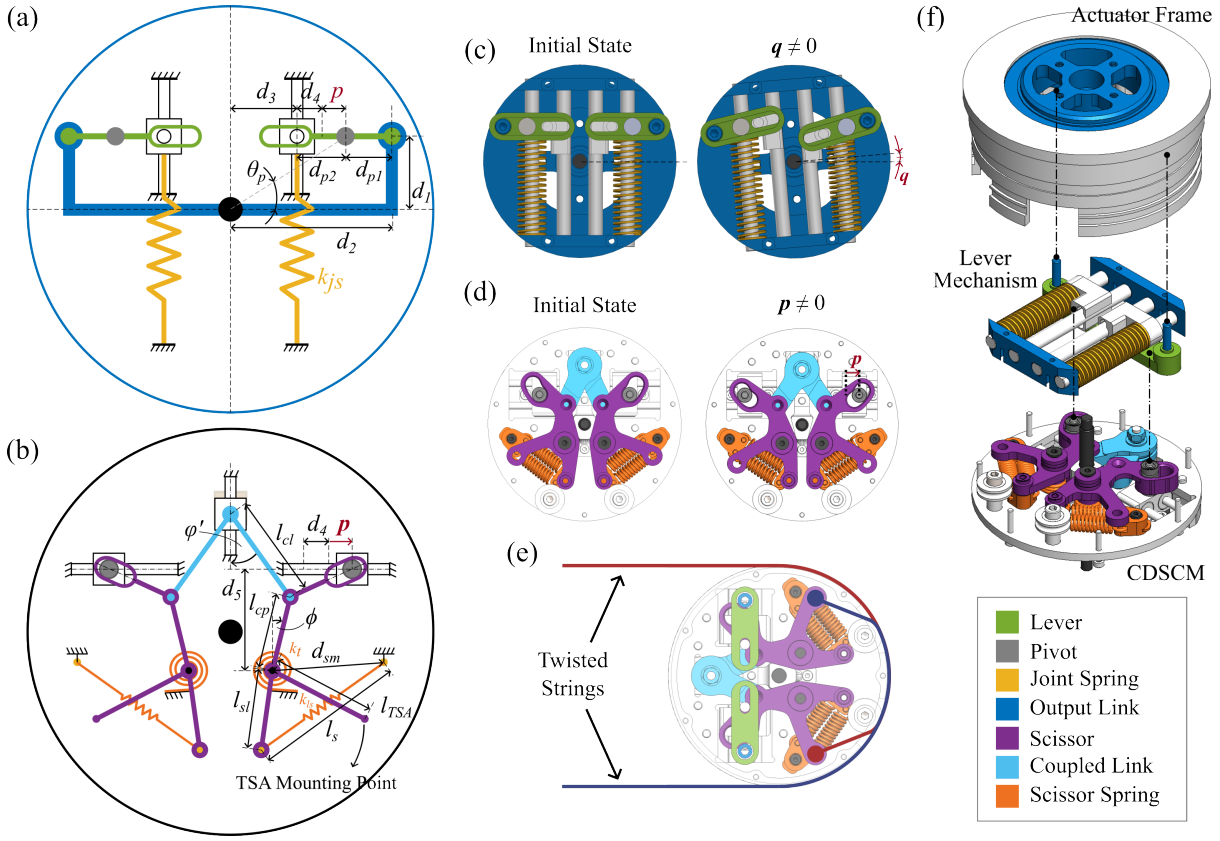

Fig. 1: Visualization of the proposed mechanism schematic diagrams and its working principle. (a) and (b) are the schematic diagram of the offset lever mechanism and the CDSCM, respectively. (c) and (d) are the demonstration of deflected lever mechanism and expanded CDSCM, respectively. (e) is the TSA routing path of the TSA in the mechanism, and (f) is the explode view of the VSM. A color legend of the components in the VSM is showed on the bottom right corner.

aligns with the initial lever orientation. In addition, the slot profile is designed to establish a linear relationship between the input link angular velocity and the pivot linear velocity.

The offset (double-track) lever mechanism and the CDSCM are assembled as shown in Fig. 1(f) to construct the proposed VSM. Each open-end of the aTSA is connected to its corresponding TSA mount and routed along a machining groove on the Actuator frame, as shown in Fig. 1(e). Sufficient pretension is provided to each Twisted String Actuator by springs on the input link of CDSCM to ensure proper actuation performance. When the CDSCM is antagonistically pulled by twisting both TSAs, the pivot heads travel in the lever slots away from each other, causing the CDSCM springs to store elastic energy. This process is called expansion, as shown in Fig. 1(d). On the contrary, untwisting both TSAs allows the CDSCM springs to release their stored energy, returning the pivots to their initial positions. This process is called retraction. To overcome external load at the pivot during expansion and retraction, the design parameters are chosen to maximize the force at the pivots through minimization of d_5 and adjustment of l_{sm} and l_{sl}. Furthermore, l_{TSA} is maximized to reduce the force required for CDSCM expansion. The remaining parameters are fixed geometric values, defined in Table. I.

III. MATHEMATICAL BACKGROUND

This section is organized into two parts: 1) stiffness modeling and 2) the CDSCM force relation. The stiffness profile of the proposed offset lever mechanism is derived to estimate joint compliance across the active pivot range and allowable deflection range. To identify an actuator suitable for expanding and holding the CDSCM mechanism during experimentation, the CDSCM force relation under static conditions is solved to determine the minimum required TSA tension. The model is formulated based on the following assumptions: 1) All friction are negligible; 2) Every component is rigid and have no deflection; and 3) The joint springs allows only compression force because the compression springs are employed in the prototype.

A. VSM Stiffness Modeling

When τ_{ext} is applied to the output link, elastic energy is stored in the joint springs, as shown in Fig. 2. The elastic torque of the joint can be formulated as

$$\tau_j = \frac{d}{dq} E_j = \frac{1}{2} \sum_{n=1}^{n_s} k_{js_n} \Delta x^2(p, q, \gamma_n) \tag{1}$$

where τ_j is the elastic torque of the joint, E_j is the elastic energy stored in the joint, and q is the joint deflection. Since

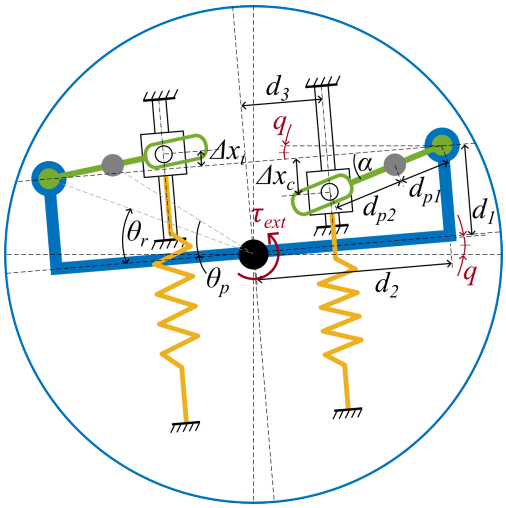

Fig. 2: The schematic diagram showing the kinematic relation of the offset lever mechanism when deflected by external load, τ_{ext}.

the linear springs are employed as the main compliance elements, the joint elastic energy E_j can be formulated by using Hook's law, where k_{js} is the stiffness of each spring in the joint. $\Delta x(p, q, \gamma)$ denote the linear spring deflections as a functions of the pivot position p, joint deflection q, and spring configuration γ. For compression side $\gamma = 1$ and tension side $\gamma = -1$. In our prototype, tension side is not present as assumed. From the geometric relations in Fig. 2, Δx is derived as follows:

$$\Delta x(p, q, \gamma) = (d_2 - d_3)\tan(\alpha(p, q, \gamma)) \tag{2}$$

$$\alpha(p, q, \gamma) = \arctan\left(\frac{\gamma(d_1 - \sqrt{d_1^2 + (p + d_3)^2}\,\sin(\theta_p(p) - \gamma q))}{d_2 - \sqrt{d_1^2 + (p + d_3)^2}\,\cos(\theta_p(p) - \gamma q)}\right) \tag{3}$$

where θ_p and can be calculated by $\arctan\left(\frac{d_1}{d_3+p+p_i}\right)$, and d_1, d_2, and d_3 are fixed geometric parameters. The $\alpha(p, q, \gamma)$ is the angle between the lever and output link as shown in Fig. 2. Combining Eq. 1–3, the elastic torque is obtained as a function of p, q, and γ, thus the joint stiffness $k_j(p, q, \gamma)$ is expressed as

$$k_j(p, q, \gamma) = \frac{d}{dq}\tau_j(p, q, \gamma) \tag{4}$$

According to Eq. 4, the VSM can achieve a minimum stiffness of 9.8 Nm/rad, with the maximum stiffness of ∞ Nm/rad. The estimated stiffness surface is presented in Fig. 3.

B. Force Relation in CDSCM

When the VSM stores elastic energy, the force from the joint springs is transmitted to the pivots via the lever through the CDSCM kinematics, resulting in CDSCM retraction. To counteract this force and maintain the pivot positions, sufficient tension must be provided by each TSA at the respective TSA mounting points on the input link.

For simplification, a new generalized coordinate, ϕ, is introduced, representing the angle between the vertical axis

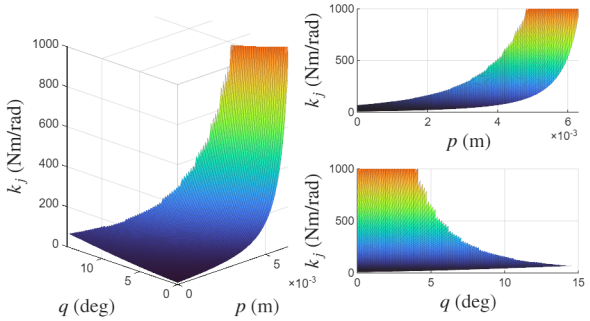

Fig. 3: The stiffness surface plot of the proposed VSM, when the joint spring stiffness is 5900 N/m.

of the VSM base and the input link. The input link slot design defines the linear relationship between ϕ and p, which is expressed as Jacobian J_p^{ϕ}. Thus, we can formulate the relationship between ϕ and p as $d\phi = J_p^{\phi} dp$.

The required TSA tensions on the left and right sides, $T_{\text{TSA}_{L,R}}$, for maintaining the pivot positions under loaded conditions, are determined through static analysis with the VSM base fixed in the experimental setup. For simplification, every rigid body is modeled as a weightless link, allowing us to neglect the inertial effects. The resultant torque of the input link is expressed as follows:

$$\sum \tau_{in} = \tau_{F_{TSA}} - \tau_s - \tau_{F_{p_H}} - \tau_{cl} \tag{5}$$

The subscripts of τ represent the following: in for the input link, F_{TSA} for the TSA tension at the mounting point, s for the springs, F_{p_H} for the pivot force along the horizontal axis of VSM base, and cl for the coupled link. The $\tau_{F_{p_H}}$ is generated by the joint spring transmitted via the lever and constrained by the pivot slider. The magnitude of force at the pivot can be calculated using the following equation:

$$F_p(p, q, \gamma) = \frac{d_{p_1} + d_{p_2}}{d_{p_1}}(k_{js}\Delta x)\cos(\alpha) \tag{6}$$

$$F_{p_H}(p, q, \gamma) = F_p \sin(\alpha + q) \tag{7}$$

The distances from the pivot to the force point and spring slider are denoted by d_{p_1} and d_{p_2}, respectively. Δx and α are obtained from Eq. 2-3. All variables are functions of p, q, and γ. The values of d_{p_1} and d_{p_2} are derived from the geometric relations, illustrated in Fig. 2, as follows:

$$d_{p_1}(p, q, \gamma) = \sqrt{(r\cos(q + \theta_r) - (p + d_3))^2 + (r\sin(q + \theta_r) - \gamma d_1)^2} \tag{8}$$

$$d_{p_2}(p, q, \gamma) = \frac{d_2 - d_3}{\cos(\alpha)} - d_{p_1} \tag{9}$$

where r and θ_r can be calculated by $\sqrt{d_1^2 + d_2^2}$ and $\arctan\left(\frac{d_1}{d_2}\right)$, respectively. To convert the pivot force, F_{p_H}, into a input link torque, τ_{P_H}, the Jacobian, J_p^{ϕ}, with the virtual work principle under static conditions ($\delta W = 0$) are used for formulating the following relation:

$$\tau_{F_{p_H}} = J_p^{\phi -1} F_{p_H} \tag{10}$$

The total spring torque, τ_s, in each input link is a combination of the torque from linear spring , τ_{ls}, and torsional spring, τ_{ts}, as follows:

$$\tau_s = \tau_{ls} + \tau_{ts} \tag{11}$$

$$\tau_{ls}(\phi) = (k_{ls}\Delta x_{ls}) l_{sl} \sin(\theta_{sm}) \tag{12}$$

$$\tau_{ts}(\phi) = k_t(\phi_i + (\Delta\phi) \tag{13}$$

where Δx_{ls} and θ_{sm} are the deflection of the linear spring and the angle between linear spring and the spring mounting part of input link, respectively. Both are functions of ϕ and can be kinematically determined from geometric variables shown in Fig. 4. Similar considerations apply to θ_{TSA}, the angle between the TSA mounting part of the input link and the TSA, which is used for determining the torque generated by the TSA tension, $\tau_{F_{TSA}}$, as shown below.

$$\tau_{TSA} = F_{TSA} \cos(\theta_{TSA}) \cdot l_{TSA} \tag{14}$$

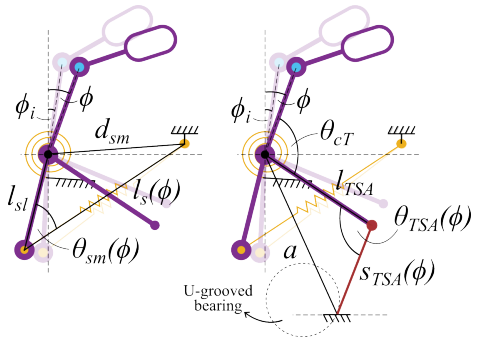

Fig. 4: The schematic of the input link geometry for calculating τ_s and τ_{TSA}. The left figure illustrates the relationship between l_{sl}, d_{sm}, $l_s(\phi)$, and $\theta_{sm}(\phi)$, while the right figure shows the relationship between a, l_{TSA}, $s_{TSA}(\phi)$, and $\theta_{TSA}(\phi)$.

The torque from the coupled link τ_{cl} occurs whenever one of the input links is not in the statics equilibrium by considering the combination of τ_{TSA}, τ_s, and τ_{p_H} on the input link. The extra force pass through the coupled link to the couple slider. At the coupled crank, the coupled link forces, F_{cl}, from both input links interact, coupling two separate slider-crank mechanisms into a single mechanism to produce a unified output. Thus, the force relation at the coupled crank can be formulated as follows:

$$\sum F_{c_V} = F_{c_{V_R}} + F_{c_{V_L}} \tag{15}$$

$$F_{c_{V_{L,R}}} = F_{cl_{L,R}} \sin(\phi) \tag{16}$$

$$\tau_{cl_{L,R}} = \frac{F_{c_{V_{L,R}}} l_{cp}}{\sin(\phi)} \tag{17}$$

where F_{c_V} is the force at coupled crank on the vertical axis of the VSM base. L, R denote the left and right input link. From Eq. 5–17, two key mathematical expressions can be formulated.

$$[F_{TSA_L}, F_{TSA_R}] = f(p, q, \Delta F_{TSA}) \tag{18}$$

$$F_{TSA_{R,L}} = f(p, q, F_{TSA_{L,R}}) \tag{19}$$

Eq. 18 is for calculating left and right TSA tension to maintain the pivot position while controlling the output torque by inputting the VSM states, p and q, and the tension differences, ΔF_{TSA}. Eq. 19 is for calculating single side TSA tension, $F_{TSA_{L,R}}$, by given the VSM states, p and q, and the other side TSA tension, $F_{TSA_{R,L}}$. By considering one side of the TSA as having zero tension, the obtained $F_{TSA_{L,R}}$ is used to select appropriate TSA and motor parameters, ensuring sufficient tension to maintain the pivot position under loaded VSM conditions, based on the kinematic model proposed in [14], as follows:

$$F_{TSA} = \frac{\sqrt{L_{TSA}^2 - (r_{TSA}\theta_m)^2}}{r_{TSA}^2 \theta_m} \tau_m \tag{20}$$

where L_{TSA} is the TSA length, r_{TSA} is the TSA radius, θ_m is the motor angular position and τ_m is the motor torque.

TABLE I: The value of the VSM design parameters.

parameters	Value	parameters	Value
d_1 (mm)	12	d_2 (mm)	26.5
d_3 (mm)	11	d_4 (mm)	19.5
p_i (mm)	8.2	l_{cp} (mm)	15.3
l_{TSA} (mm)	20	l_{sl} (mm)	15.3
l_{cl} (mm)	17.5	d_{sm} (mm)	21.5
$l_s(\phi_i)$ (mm)	20	k_{js} (N/m)	5900
k_t (Nm/rad)	0.21	k_{ls} (N/m)	3430
a (mm)	27.32	θ_{cT} (rad)	1.8127
$s_{TSA}(\phi_i)$ (mm)	18.61	L_{TSA} (mm)	250
r_{TSA} (mm)	1.2	ϕ_i (rad)	0.1527
J_p^ϕ	31.746		

IV. PROTOYTPE AND EXPERIMENT SETUP

A prototype of the designed VSM was manufactured from CNC-milled aluminum and stainless steel for experimental evaluation, while only the base fixture parts are 3D-printed, as shown in Fig. 5. Each revolute joint and slider has deep-groove ball bearings or linear bushings with shafts to support and constrain motion, ensuring stability and minimal energy loss at minimal cost. The prototype can achieve 0.5 kg mass and 84 mm diameter without the joint bearing. The actuator specifications are provided in Table II.

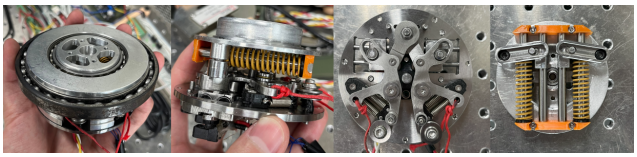

Fig. 5: The fabricated VSM prototype.

The prototype is operated using the experimental setup shown in Fig. 6. Two geared DC motors (ZHENGKE

ZGX38REE) are employed as the TSA driving units, and and 1.2 mm Dyneema braided strings are used as the string for TSA. Each TSA has a load cell and a linear rail block attached at its open-end side to measure the tension and support the motion. Another side of the load cell connects with another string to transmit tension to the VSM at the string mounting point. Two linear encoders (HEDS9730) are mounted on the pivots to track their positions. A high-torque smart actuator (GYEMS RMDX-8 Pro), communicating via a 1 MHz CAN protocol, is attached to the output link to apply external torque and measure deflection and current back. The VSM is rigidly fixed to the testbed to simplify experimental procedures. The controller of the setup (Teensy 4.1) receives a sequence of predefined experiment state commands from a scheduler script running on a PC via USB serial communication. The VSM states are regulated by a PID control framework, with distinct parameters defined for each experimental state. Experimental data were transmitted back to the PC via the same USB connection using the JSON protocol at 50 Hz and post-processed in MATLAB.

TABLE II: The specifications of proposed VSM.

VSM specifications	Value
Maximum pivot position, p_{max} (mm)	7.3
Joint deflection angle range for the minimum stiffness condition (°)	± 15
Theoretical stiffness range (Nm/rad)	9.8 - ∞
Stiffness regulation time (ms)	0.618
Maximum elastic energy (single joint spring: J)	0.9
VSM diameter (mm)	84
VSM thickness (mm)	50.2
VSM weight (kg)	0.5
VSM with joint bearing weight (kg)	0.65

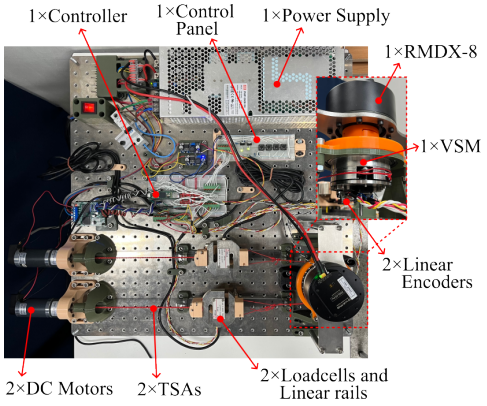

Fig. 6: Top-view of the experiment setup.

V. EXPERIMENT RESULTS AND DISCUSSION

A. Pivot regulation experiment

The ability to modify joint stiffness under different conditions is a key function of the VSM. This experiment evaluated the pivot regulation performance of the novel CDSCM mechanism driven by an antagonistic open-end tendon actuator. The pivots were initialized at zero and regulated to 36% and 73% of the maximum pivot position by the aTSA with step inputs, while applying 0 and 1 Nm external loads at the output link by the smart actuator. Pivot positions were recorded and analyzed to determine rise time. Each experiment was repeated 10 times, and the collected data are visualized in Fig. 7.

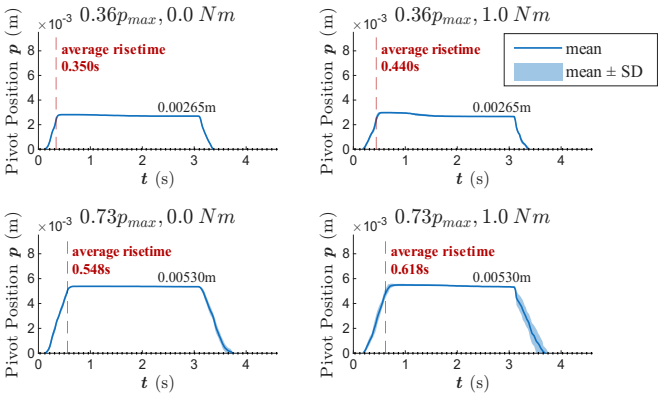

Fig. 7: The regulated pivot position profile under different load conditions and targeted stiffness value.

The dashed line indicates the desired setpoint at each timestamp, while the blue line and shaded area represent the mean and standard deviation of the logged data. The maximum regulation time was 0.618 ms for 0–73% pivot position under a 1.0 Nm load, and the minimum time was 0.35 ms for 0–50% pivot position under no load. Higher load and stiffness levels led to slower CDSCM expansion and less accurate CDSCM retraction. Uncertainty in pivot motion was observed during CDSCM retraction under loaded conditions, particularly in the final experiment, as shown by the largest shaded area during the retraction phase in Fig. 7. From the observation, the load creates an unexpected small deflection at the slider support under each pivot, disturbing the retraction from the springs.

B. Torque-deflection profile identification

The accuracy of the VSM stiffness model was evaluated through a torque–deflection profile identification experiment. The setup followed a sequence of stiffness regulation and VSM loading/unloading. During stiffness regulation, the aTSA regulated the pivots from 0–73% of the active range in eleven equally spaced increments. At each iteration, the smart actuator ramped from 0 Nm to 4 Nm and returned 0 Nm with a constant speed of 0.33°/s, which stopped every 0.5° increment to read and record the torque value. The experiment was repeated for 4 times and the results are shown in Fig. 10.

The measured torque is visualized in two phases, loading (red) and unloading (blue), to illustrate VSM torque hysteresis. The grey dashed and black dotted plots represent the raw (unscaled) and scaled estimated torque profiles, respectively. The raw (unscaled) estimated torque shows a large mismatch, as measured torque is lower than predicted when the smart actuator regulate its position. Significant excess deflection within the internal mechanism is more

severe than the previous experiment due to the higher applied load. Despite, we added 3D printed small fixtures to minimize the deflection of pivot slider supports, but the result did not change significantly. This shows that rigidity issues caused by not only the pivot slider but also other components in the offset lever mechanism. We preliminary address this issue using the series-connected stiffness concept. A constant gain C, which calculated as the ratio of maximum measured torque to maximum estimated torque, was applied at each stiffness level to compensate for structural stiffness effects. The modified model is constructed as follows:

$$\tau_j = \frac{1}{C}\left(\frac{d}{dq}E_j\right) \tag{21}$$

After applying the distinct gain to each estimated stiffness profile, the scaled estimated torque profile shows a trend matching the measured torque profile. The calculated RMSE varies below 0.274 Nm. The gain exhibits a slight nonlinear increase across the iterated stiffness levels, as shown in Fig. 8. A larger gain indicates a greater influence of structural stiffness to the system. So, the maximum achievable stiffness calculated from measured torque-deflection profile at 73% of the active pivot range is 99.26 Nm/rad.

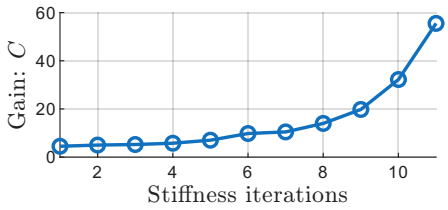

Fig. 8: The constant gain value across all stiffness iterations.

Currently, the structural stiffness has not been explicitly determined due to limitations of the VSM and the experimental setup. Therefore, a physical model that accurately represents the phenomenon in the internal mechanism cannot yet be formulated. However, the experimental results suggest that the desired profile can be achieved with sufficiently rigid and accurate fabrication, as the measured profile trend is already valid. The deflection and friction of the internal mechanism also contribute to significant energy loss during the unloading phase, leading to the torque hysteresis shown in Fig. 10.

To analyze the design and guide the future improvements, we use SolidWorks static analysis (FEA) to preliminary visualize the deflection of the internal mechanism while handling the external load. The connections between components in the simulation are defined based on realistic interaction including rigid, contact, and spring connections, except for the bolt joint which is defined as rigid connection due to the unknown pre-loading torque during prototype assembly. The simulation result is shown in Fig. 9. The right figure shows that the external torque cause the pivot and lever to twist and lean forward, producing an additional deflection at the output link. The main causes are the improper sizing of the pivot slider support shaft and the lever force point shaft. Moreover, the extra deflection in the fabricated prototype may also result from internal clearances between components and the input link which is not always rigid as assumed in the simulation.

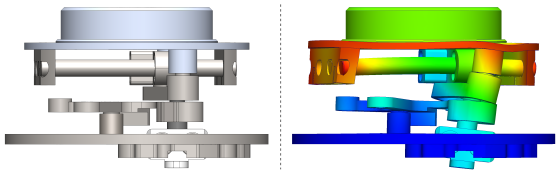

Fig. 9: The comparison between the CAD model used for displacement analysis and the resultant displacement (URES) obtained from the SolidWorks static analysis (FEA), with a deformation scale of 77.5936.

VI. CONCLUSION

In this work, we present a novel pivot-regulating mechanism, the Coupled Dual Slider Crank Mechanism (CDSCM), integrated with the offset lever mechanism Variable Stiffness Module (VSM) and antagonistic Twisted String Actuators (aTSA). The proposed VSM successfully satisfies the design objectives by relocating actuators away from the lever mechanism based VSM, allowing the pivot regulation via antagonistic pulling, and achieving 0.5 kg with 84 mm diameter and 50.2 mm thickness. The overall specification of the VSM is compared with other VSMs in Table. III. The design was evaluated through two experiments: 1) pivot regulation under loaded and unloaded condition, and 2) the evaluation VSM torque–deflection model accuracy. The torque-deflection identification result shows the right stiffness trend with the rigidity issue. Thus, our future work will focus on enhancing mechanical rigidity, reduce internal friction, modify the lever mechanism to increase the elastic energy storage capability and deflection angle, developing a full dynamic actuator model with a controller, and conducting the simultaneous position-stiffness tracking experiment.

ACKNOWLEDGMENT

The authors would like to express sincere appreciation to Prof. Jee-Hwan Ryu, Mr. Eui-Bin Shin, Mr. Hyeon-Seok Seong, and other lab members from the Interactive Robotic Systems Laboratory, KAIST, for their valuable discussions and feedback and thanks the financial supports from King Mongkut's University of Technology Thonburi (KMUTT), Thailand Science Research and Innovation (TSRI), and the National Science, Research and Innovation Fund (NSRF) (Fundamental Fund under Grant 4863167).

REFERENCES

[1] A. Bicchi and G. Tonietti. Fast and "Soft-Arm" Tactics. *IEEE Robotics & Automation Magazine*, 11(2):22–33, June 2004.

[2] S. Haddadin, A. Albu-Schäffer, and G. Hirzinger. Safety Evaluation of Physical Human-Robot Interaction via Crash-Testing. In Wolfram Burgard, Oliver Brock, and Cyrill Stachniss, editors, *Robotics: Science and Systems III*, page 0. The MIT Press, January 2008.

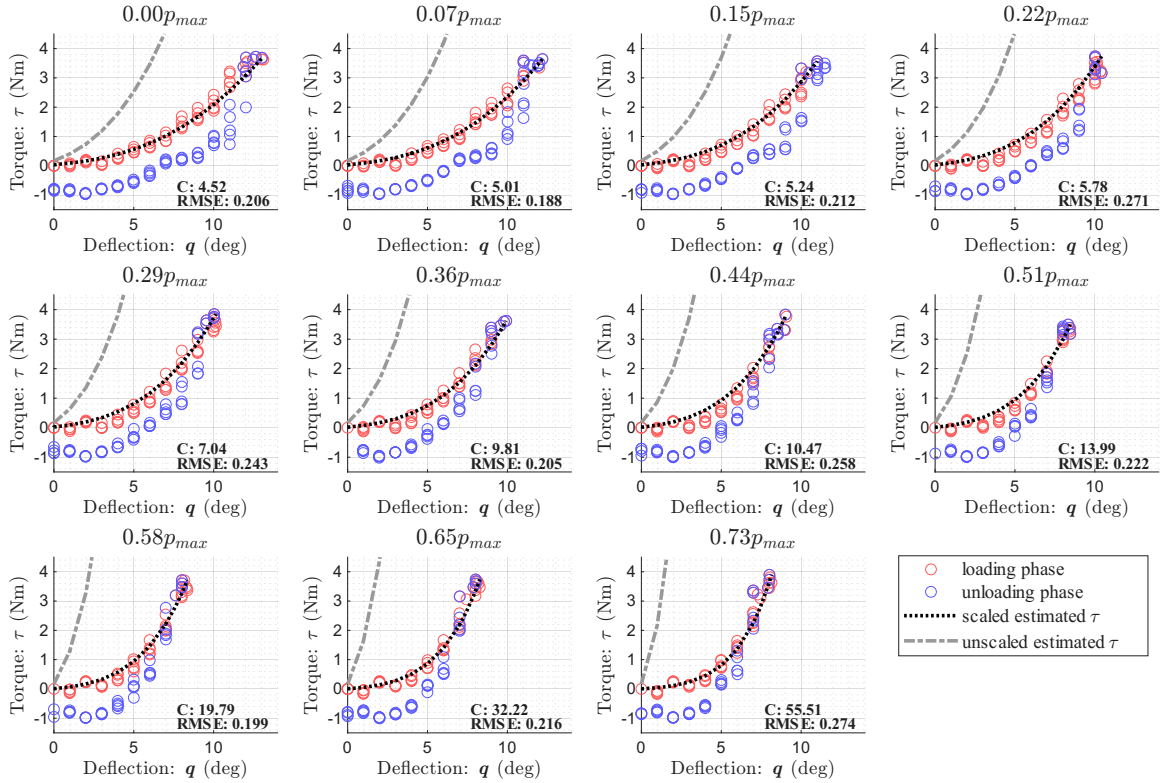

Fig. 10: Comparison of the torque measured from the prototype with the unscaled and scaled torque estimated torque from the model with respect to the input deflection (torque-deflection profile) of the proposed VSM.

TABLE III: Comparison of the specifications of VSAs with lightweight VSM

Name	description	mass (kg)	diameter (mm)	stiffness variation range (Nm/rad)	stiffness regulation time (s)	Deflection range (°)	elastic energy storability (J)
SVSA-II [13]	independent setup with lever mechanism	0.867	110	0 - ∞ (theoretically)	0.12	$\pm$39.6	-
LVSA [12]	independent setup with a pulley and FS2C	0.41	-	0 - 988	0.22	$\pm$25	-
Proposed VSM	antagonistic setup with lever mechanism	0.5	84	9.8 - 99.26	0.618	$\pm$15	0.9

[3] J.-J. Park, H.-S. Kim, and J.-B. Song. Safe robot arm with safe joint mechanism using nonlinear spring system for collision safety. In *2009 IEEE International Conference on Robotics and Automation*, pages 3371–3376, Kobe, May 2009. IEEE.

[4] S. Haddadin, A. Albu-Schäffer, O. Eiberger, and G. Hirzinger. New insights concerning intrinsic joint elasticity for safety. In *2010 IEEE/RSJ International Conference on Intelligent Robots and Systems*, pages 2181–2187, Taipei, October 2010. IEEE.

[5] S. Wolf et al. Variable Stiffness Actuators: Review on Design and Components. *IEEE/ASME Transactions on Mechatronics*, 21(5):2418–2430, October 2016.

[6] G. Grioli et al. Variable stiffness actuators: The user's point of view. *The International Journal of Robotics Research*, 34(6):727–743, May 2015.

[7] B. Vanderborght et al. Variable impedance actuators: A review. *Robotics and Autonomous Systems*, 61(12):1601–1614, December 2013.

[8] D. Popov, I. Gaponov, and J.-H. Ryu. Towards variable stiffness control of antagonistic twisted string actuators. In *2014 IEEE/RSJ International Conference on Intelligent Robots and Systems*, pages 2789–2794, Chicago, IL, USA, September 2014. IEEE.

[9] G. Palli, M. Hosseini, L. Moriello, and C. Melchiorri. Modeling and identification of a variable stiffness joint based on twisted string actuators. In *2015 IEEE/RSJ International Conference on Intelligent Robots and Systems (IROS)*, pages 1757–1762, Hamburg, Germany, September 2015. IEEE.

[10] H.-S. Seong, D.-H. Kim, I. Gaponov, and J.-H. Ryu. Development of a Twisted String Actuator-based Exoskeleton for Hip Joint Assistance in Lifting Tasks. In *2020 IEEE International Conference on Robotics and Automation (ICRA)*, pages 761–767, Paris, France, May 2020. IEEE.

[11] D. Popov, I. Gaponov, and J.-H. Ryu. Bidirectional elbow exoskeleton based on twisted-string actuators. In *2013 IEEE/RSJ International Conference on Intelligent Robots and Systems*, pages 5853–5858, Tokyo, November 2013. IEEE.

[12] C. Wang et al. A Lightweight Series Elastic Actuator With Variable Stiffness: Design, Modeling, and Evaluation. *IEEE/ASME Transactions on Mechatronics*, 28(6):3110–3119, December 2023.

[13] J. Sun, Z. Guo, D. Sun, S. He, and X. Xiao. Design, modeling and control of a novel compact, energy-efficient, and rotational serial variable stiffness actuator (SVSA-II). *Mechanism and Machine Theory*, 130:123–136, December 2018.

[14] S.-R. Lee, D. Lee, Y. Kim, and D. Shin. A compact high-torque twisted string actuator using parallel bundle-driven actuation with an asymmetric behavior compensator. *IEEE/ASME Transactions on Mechatronics*, 27(2):834–845, 2022.

[15] M. Tavakoli, R. Batista, and P. Neto. A compact two-phase twisted string actuation system: Modeling and validation. *Mechanism and Machine Theory*, 101:23–35, 2016.